Biochimica et Biophysica Acta 1817 (2012) 445–452

Contents lists available at SciVerse ScienceDirect

Biochimica et Biophysica Acta

journal homepage: www.elsevier.com/locate/bbabio

# Red antenna states of Photosystem I trimers from *Arthrospira platensis* revealed by single-molecule spectroscopy

Marc Brecht [a,*], Martin Hussels [a], Eberhard Schlodder [b], Navassard V. Karapetyan [c]

[a] Institut für Physikalische und Theoretische Chemie, Eberhard-Karls-Universität Tübingen, Auf der Morgenstelle 18, 72076 Tübingen, Germany
[b] Max-Volmer-Laboratorium für Biophysikalische Chemie, Technische Universität Berlin, Strasse des 17, Juni 135, 10623 Berlin, Germany
[c] A.N. Bakh Institute of Biochemistry, Russian Academy of Sciences, Leninsky Prospect 33, 119071 Moscow, Russia

ARTICLE INFO

*Article history:*
Received 18 October 2011
Received in revised form 21 November 2011
Accepted 23 November 2011
Available online 3 December 2011

*Keywords:*
Photosystem I
Single-molecule spectroscopy
Long-wavelength antenna chlorophyll
Energy transfer
*Arthrospira platensis*

ABSTRACT

Single-molecule fluorescence spectroscopy at 1.4 K was used to investigate the spectral properties of red (long-wavelength) chlorophylls in trimeric Photosystem I (PSI) complexes from the cyanobacterium *Arthrospira platensis*. Three distinct red antenna states could be identified in the fluorescence spectra of single PSI trimers from *A. platensis* in the presence of oxidized P700. Two of them are responsible for broad emission bands centered at 726 and 760 nm. These bands are similar to those found in bulk fluorescence spectra measured at cryogenic temperatures. The broad fluorescence bands at ≅726 and ≅760 nm belong to individual emitters that are broadened by strong electron–phonon coupling giving rise to a large Stokes-shift of about 20 nm and rapid spectral diffusion. An almost perpendicular orientation of the transition dipole moments of F726 and F760 has to be assumed because direct excitation energy transfer does not occur between F726 and F760. For the first time a third red state assigned to the pool absorbing around 708 nm could be detected by its zero-phonon lines. The center of the zero-phonon line distribution is found at ≅714 nm. The spectral properties of the three red antenna states show a high similarity to the red antenna states found in trimeric PSI of *Thermosynechoccocus elongatus*. Based on these findings a similar organization of the red antenna states in PSI of these two cyanobacteria is discussed.

© 2011 Elsevier B.V. All rights reserved.

## 1. Introduction

Photosystem I is a large pigment-protein complex embedded in the thylakoid membrane. It is one of the major protein complexes catalyzing the primary reactions of oxygenic photosynthesis. After photoexcitation, PSI transports electrons from reduced plastocyanin or cytochrome $c_6$ on the luminal side to ferredoxin on the stromal side of the photosynthetic membrane [1]. PSI of higher plants and algae (named PSI-200) consists of the PSIcore complex and the peripheral light-harvesting complex LHC I. In cyanobacteria only the core complex exists. Even though the PSI core complex from cyanobacteria [2,3] differs in organization and polypeptide content to that of higher plants [4] and algae, the structures are very similar to each other [5]. The PSI core complex coordinates all of the redox cofactors and the core antenna of ~100 chlorophyll *a* (Chl) and ~20 ß-carotene molecules. After absorption of light by an antenna pigment, the excitation energy is efficiently trapped within about 30 ps via charge separation in the reaction center leading to $P700^+A_0^-$. Charge stabilization is achieved by subsequent electron transfer to the secondary acceptor $A_1$, then further to $F_X$ and finally to the terminal electron acceptors $F_A$ and $F_B$.

A fascinating feature of the core antenna of cyanobacterial PSI is the presence of several Chl molecules absorbing at longer wavelength (lower energy) than P700. These red-shifted Chls are often referred to as red Chls or long-wavelength Chls (LWC) (for reviews, see Karapetyan et al. [6,7] and Gobets and van Grondelle [8]). Long-wavelength Chls of PSI from different cyanobacteria show remarkable differences concerning the number and the spectral positions (see Table 1). The spectral heterogeneity of the antenna Chls can be explained by site-energy differences arising from pigment–protein interactions and strong pigment–pigment interactions of excitonically coupled Chls. LWCs have a pronounced effect on the energy transfer within the whole antenna system. The excited states in the antenna tend to achieve a Boltzmann distribution among the different spectral forms before trapping. Excitation energy transfer processes from the bulk to LWCs occur within a few ps (see [6–8] and references therein). As a consequence, fluorescence is emitted mainly from the LWC and trapping becomes an energetically uphill process that is enabled by thermal energy of the surrounding. At physiological temperatures, thermal energy is sufficiently available and the quantum yield of photochemistry is virtually independent of the wavelength of the excitation, even at wavelengths of up to

*Abbreviations:* $A_0$, primary electron acceptor in PSI; $A_1$, secondary electron acceptor in PSI (a phylloquinone); Chl *a*, chlorophyll *a*; Cxxx, Chl absorbing at xxx nm; FeS, iron-sulfur-cluster; $F_X$, $F_A$ and $F_B$, three [4Fe-4S] clusters in PSI; Fxxx, fluorescence with an emission maximum at xxx nm; FWHM, full width at half maximum P700 ($P700^+$), primary electron donor of PSI in the reduced (oxidized) state; PSI (PSII), photosystem I (photosystem II); PW, phonon-wing; ZPL, zero-phonon line

* Corresponding author. Tel.: +49 7071 29 76239.
*E-mail address:* marc.brecht@uni-tuebingen.de (M. Brecht).

0005-2728/$ – see front matter © 2011 Elsevier B.V. All rights reserved.
doi:10.1016/j.bbabio.2011.11.012

**Table 1**
Comparative analysis of ZPL of red Chl forms in PSI trimers from the various cyanobacteria.

| Cyanobacteria | Absorbance bands (amount of Chls) | P700 fluorescence $\lambda_{max}$ | $P700^+$ fluorescence $\lambda_{max}$ | ZPL distribution $\lambda_{max}$ |
|---|---|---|---|---|
| *A. platensis* | 708 (7–8) [7,12]<br>740 (3) [7,12] | 760 [7,37] | 727 [9] | 714 |
| *T. elongatus* | 708 (5–6) [7,12]<br>719 (4–5) [7,12] | 735 [13] | 731 [13] | 710 [27] |
| *Synechocystis sp.* PCC 6803 | 708 (5) [7,8] | | 722.5 [37] | 699 [38]<br>710 [38] |
| *Synechococcus sp.* PCC 7002 | 703 (2) [39] | | 714 [39] | 698 [39] |

760 nm [9]. At lower temperatures, however, the LWCs act as irreversible traps for eexcitation energy, thereby decreasing the quantum efficiency of charge separation and increasing the fluorescence yield [9].

PSI trimers of *Arthrospira platensis* contain the reddest Chl antenna state reported so far, absorbing at 740 nm (C740) and emitting at 760 nm (F760) at cryogenic temperatures [10–12]. The deconvolution of 5 K absorption spectra of trimeric PSI yields two red bands, one at 708 nm (C708) and the other at 740 nm (C740); the oscillator strength of these bands corresponds to 7–8 and 3 Chls, respectively [12]. The fluorescence intensity of the different red antenna states of trimeric PSI from *A. platensis* depends strongly on the redox state of P700. The 760 nm fluorescence (F760), that dominates the fluorescence spectrum of trimeric PSI with P700 in the reduced state (P700), is almost completely quenched in the presence of oxidized P700 ($P700^+$) that acts as an efficient quencher [13].

In monomeric PSI complexes of *A. platensis* the absorption band around 740 nm is lost completely [10–13] indicating that the absorption at 740 nm can be assigned to one excitonically coupled Chl aggregate localized in the trimerization domain [14,15]. The oscillator strength of the 708 nm band is similar in monomeric and trimeric PSI [16,17]. To explain the observed oscillator strength corresponding to 7–8 Chls, more than 4 aggregates (dimers or trimers) may be required. Different putative candidates for C708 have been proposed in the literature (see [6–8] and references therein). It should be noted that for most of the candidates discussed in the literature the oscillator strength is shared between the low energy exciton transition absorbing at longer wavelength around 708 nm and the high energy exciton transition absorbing at shorter wavelengths. Therefore, the oscillator strength that is contributed, for example, by a dimer to the long-wavelength absorption band, corresponds generally to less than 2 Chls.

The emission of C708 has its maximum at 726 nm in PSI containing P700 in the oxidized state ($P700^+$). Recently it was shown that an additional emitter at 731 nm is present, if P700 is in the reduced state. This emitter belongs also to one aggregate of C708 and is strongly quenched by $P700^+$ [13].

The PSI complex of the cyanobacterium *Thermosynechoccocus elongatus* is often used as a reference system for PSI, due to the well-resolved structural model from X-ray crystallography [2,3,18]. The absorption spectrum of trimeric PSI complexes from *T. elongatus* shows two absorption bands in the red region, one at 708 nm (C708) and a second at 719 nm (C719). Their oscillator strength corresponds to that of 5–6 and 4 Chls, respectively. Monomeric PSI complexes of *T. elongatus* show a reduced number of C719 Chls corresponding to the loss of 2 Chls. Therefore, it has been suggested – like for C740 – that some of these LWCs are located close to the trimerization domain of the complexes [9,14,15]. With hole-burning experiments it was shown that the description of the spectral properties of the absorption profile cannot sufficiently be described solely by the pools C708 and C719, therefore a third spectral form with absorption maximum at 715 nm (C715) was introduced [19]. The fluorescence spectra of PSI of *T. elongatus* at 77 K exhibit one broad emission band [13]. The wavelength position and the integral intensity of this band are different for monomeric and trimeric PSI complexes and depend on the redox state of P700. The fluorescence spectra indicate at least three emitters with maximum emission at 730, 734 and 739 nm. The emission at 739 nm is only observable in PSI trimers containing P700 in the reduced state, because the emission of F739 is highly quenched by $P700^+$. In PSI monomers F739 is not observed, therefore it can be associated with the two Chl's of C719 that are not present in monomeric PSI. An additional weak emitter close to 710 nm was found by single-molecule spectroscopy. It was assumed that this emitter belongs to the C708 pool [20,21].

With single-molecule spectroscopy it is possible to observe the fluorescence of PSI down to the level of single trimers or monomers [20]. At the single-molecule level spectral properties are accessible, which are averaged out in large ensembles [22]. The fluorescence of single PSI complexes from all species studied so far is composed of various contributions from the red pool emitters. The spectral characteristics of these different Chl aggregates vary remarkably. The variations concern – besides the emission wavelength – their intensity, electron–phonon coupling, and degree of spectral diffusion. The most striking parameters in the spectra of single PSI complexes are the rate and width of spectral diffusion acting on the different emitters. If the site energies of chromophores are little affected by fluctuations (weak spectral diffusion) and if the rate of spectral diffusion is smaller than the rate of data acquisition, the emission profile of a single emitter composed of a sharp zero-phonon line (ZPL) and its phonon-wing (PW) becomes observable in the spectra. Induced by the remaining fluctuations at low temperature, spectral jumps of these ZPLs can be observed [23].

The width of these jumps can extend up to several nanometers indicating remarkable changes in the site energy of the involved chromophores. If the rate of spectral diffusion is higher (fast spectral diffusion) than the rate of data acquisition, only broadened lines are visible [24]. If the signature of the ZPLs is lost, it is no longer obvious whether the broadened lines are due to a single or several emitters. Then additional properties like the polarization of the emission [25] must be taken into account to deduce the number of the underlying emitting states.

In this work we focus on the fluorescence of single PSI trimers of *A. platensis* with the reddest Chl antenna state absorbing at 740 nm [6,11,12]. The presented experiments reveal the spectral properties of three different emitters in PSI of *A. platensis*.

## 2. Materials and methods

### 2.1. Preparation of samples

Trimeric PSI complexes have been isolated from the cyanobacterium *A. platensis* according to Ref. [12]. Purified complexes at a concentration of about 200 μM Chl were stored in 50 mM Tris–HCl buffer (pH 8.0) and 0.08 mM (0.04% w/v) detergent n-dodecyl ß-D-maltoside (Sigma) at −80 °C. This amount of detergent is adequate for a PSI trimer concentration of 1 μM to avoid PSI aggregation [26]. For measurements of the fluorescence of single PSI complexes, the sample was diluted in buffer solution containing 20 mM Tricine (pH 7.5), 25 mM $MgCl_2$, 4 mM n-dodecyl ß-D-maltoside, and 5 mM sodium ascorbate for prereduction of P700. The PSI containing solution was diluted to a PSI trimer concentration of ≅3 pM. Less than 1 μl of this sample was placed between two cover slips assuring spatial separation of individual PSI trimers. Sample preparation was carried out under indirect daylight. To observe the fluorescence of single PSI complexes, a home-built confocal microscope was used. The experimental setup was described recently [27]. The sample and the microscope objective were immersed in super fluid helium, with a sample temperature of 1.4 K. The excitation power measured directly behind the beam-scanning module was 100 μW, and the excitation

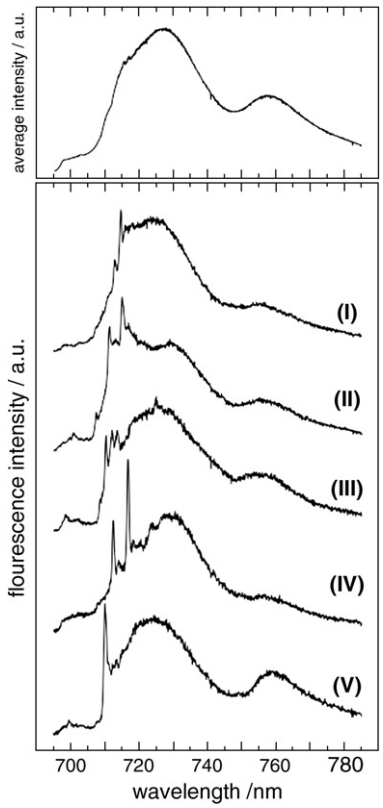


**Fig. 1.** (I)–(V): Single-molecule fluorescence spectra of PSI complexes of *A. platensis* (I–V). Spectra were recorded for different individual complexes with $\lambda_{exc} = 680$ nm at T = 1.4 K. The acquisition time was 100 s for each spectrum. Top: average of all spectra recorded (106 PSI trimers).

wavelength was 680 nm for all experiments. The stray light of the laser was suppressed by a Raman long-pass filter (AHF HQ695LP).

### 2.2. Data evaluation procedures

For data analysis we used the software package Matlab. The occurrence of ZPLs in a sequence of fluorescence spectra from individual PSI trimers has been evaluated using the following algorithm. It is based on three steps. First, the spectra series are smoothed in two dimensions (wavelength and time) using a moving average filter as provided in Matlab (Curve Fitting Toolbox). In a second step, a standard Laplace 1D edge filter is applied in the wavelength domain to enhance sharp and to suppress broad structures. In a third step, all wavelength positions are collected where the intensity surpasses a certain threshold, which implies the presence of narrow lines in the spectra. Finally, the information is collected for all PSI complexes and visualized in histograms as given in the Results section.

## 3. Results

### 3.1. Emission spectra of individual PSI trimers

Single-molecule fluorescence spectroscopy at 1.4 K was used to detect the fluorescence of single PSI complexes from *A. platensis* [20]. The emission originates from LWC, which act as traps for the excitation energy [17]. A PSI trimer concentration of 3 pM was chosen for the collection of the fluorescence of single PSI complexes from *A. platensis*. At this low concentration, the spatial separation of the trimers is much larger than the width of the confocal volume. In total, we recorded spectral information for 106 individual PSI trimers. In Fig. 1 five representative examples for fluorescence spectra of single PSI trimers (denoted I–V) together with the average spectra of all complexes (on top) are given. The spectra were scaled to similar magnitude for better comparison. The spectra of almost all complexes show ZPLs in the range <720 nm and broad intensity distributions with maxima around 725 nm and 758 nm. The broad bands can be associated with the known emission bands F726 and F760 of low temperature bulk emission spectra, therefore the respective nomenclature will be used in the following.

From all spectra of single trimers, the peak positions of F726 ($=\lambda_{F726}$) and F760 ($=\lambda_{F760}$) were derived. For this purpose, the wavelength range was divided into two regions, in which the contributions of F726 and F760 can be found: 700–740 nm and 740–780 nm. The histograms presented in Fig. 2a show the distributions of the emission band maximum wavelengths, $\lambda_{F726}$ and $\lambda_{F760}$. The full width at half maximum (FWHM) of these distributions can be estimated to be about 6 nm. This indicates that the contribution of inhomogeneous broadening (inter-complex heterogeneity) to the width of the broad emission band as observed in the ensemble spectrum (see Fig. 1) is rather small. This holds even in the case of F726 where it cannot be excluded that more than one red state contributes to the emission. Furthermore, the question was examined, whether the peak positions of F726 and

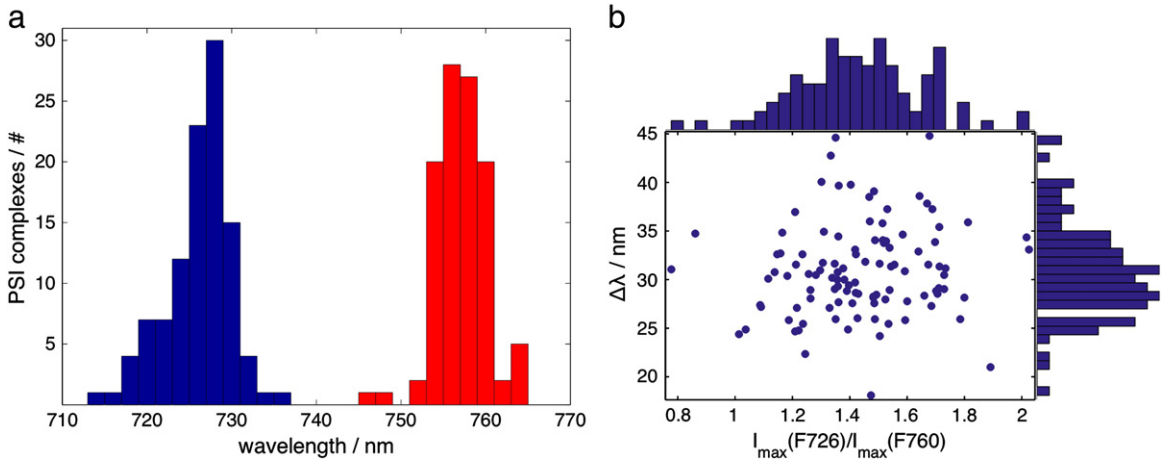


**Fig. 2.** (a) Distribution of the maxima positions found in the emission spectra of single PSI trimers from *A. platensis*. The wavelength range was divided into two regions: 700–740 nm where the F726 band is observed and 740–780 nm where the F760 band is observed. In each range the peak positions were determined and given as histograms (see also text). (b) 2D-scatter plot between the relative intensities of F726 and F760 (the intensities were derived at the respective position of the maxima) and the wavelength difference between these two emitters ($\Delta\lambda = \lambda_{F760} - \lambda_{F726}$). $\lambda_{F760}$ and $\lambda_{F726}$ are the wavelength positions of the maxima of F726 and F760 observed in the spectra of the individual PSI trimers.

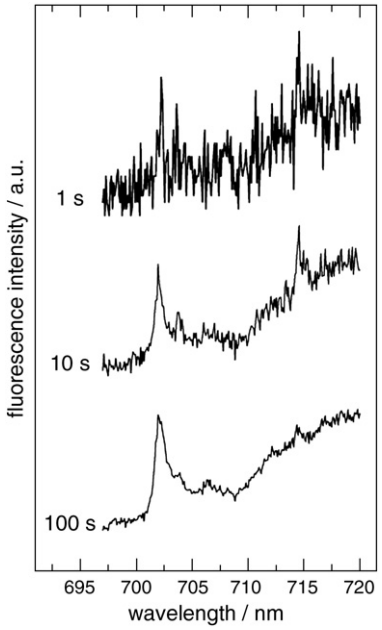


**Fig. 3.** Fluorescence spectra of a single PSI trimer from *A. platensis* measured with different acquisition times. The spectra were acquired on the same trimer in 1, 10, and 100 s as indicated. $\lambda_{exc} = 680$ nm, T = 1.4 K.

F760 in individual PSI complexes are correlated. Therefore, the peak positions $\lambda_{F726}$ were plotted versus $\lambda_{F760}$ in a 2D-scatter plot (data not shown). The plot did not reveal any correlation between the peak positions of the two broad emission bands.

The intensities of the broad bands F726 and F760 were determined for all complexes. Due to spectral overlap of the broad bands, it was not possible to determine reliably the integral intensities. Therefore, the maximum intensity $I_{max}$ was used directly from the data as a measure of the intensity. The 2D-scatter plot between the ratio $I_{max}(F726)/I_{max}(F760)$ and the wavelength difference of the peak positions ($\Delta\lambda = \lambda_{F760} - \lambda_{F726}$) in the single complex emission spectra is shown in Fig. 2b. The relative intensity $I_{max}(F726)/I_{max}(F760)$ is given on the abscissa and $\Delta\lambda$ on the ordinate. The corresponding 1D histograms are shown on the respective axes. In this representation no correlation is visible between the intensities of F726 and F760 and the energetic separation $\Delta\lambda$.

### 3.2. ZPL dynamics

Fluorescence spectra of single PSI complexes (see Fig. 1) were measured using various acquisition times to analyze the properties of the ZPLs. The dependence of the spectra of a single PSI trimer on the acquisition time is shown in Fig. 3 presenting spectra taken within 1, 10, and 100 s. In the spectrum taken within 1 s, two ZPLs at 702 nm and 715 nm are present. Due to their low intensity, these lines exceed hardly the noise level. Increasing the accumulation time yields an increase of the S/N ratio, but also a broadening of the ZPLs due to spectral diffusion. The ZPL at 702 nm broadens, but remains visible even after 100 s accumulation time, whereas the ZPL at 715 nm is almost completely lost. In similar manner we analyzed the widths of the two broad emission bands of F726 and F760. It turned out that the widths of these broad distributions (≅25 nm) remain largely unchanged when varying the acquisition time from 1 s up to 120 s (data not shown).

In order to investigate and compare the dynamics of the ZPLs in the emission spectra of single PSI trimers from *A. platensis* in more detail, sequences of fluorescence spectra were recorded for all PSI trimers. With an acquisition time of 1 s for one spectrum the S/N ratio of our setup is sufficient to monitor ZPL dynamics directly. Two examples of different dynamical behavior of ZPLs are shown in Fig. 4a, b. Sequences of 100 fluorescence spectra with an accumulation time of 1 s for each spectrum are displayed for two different single PSI trimers. The sequence in Fig. 4a shows an example for a single ZPL changing its wavelength position on the timescale of several seconds. The ZPL shows several discrete jumps of about 1 nm. In the sequence in Fig. 4b, the spectral diffusion of the ZPL is much faster. Variations of the emission wavelength occur at higher rates. The duration between two jumps is in the same order as the acquisition time. In cases where ZPLs reside on

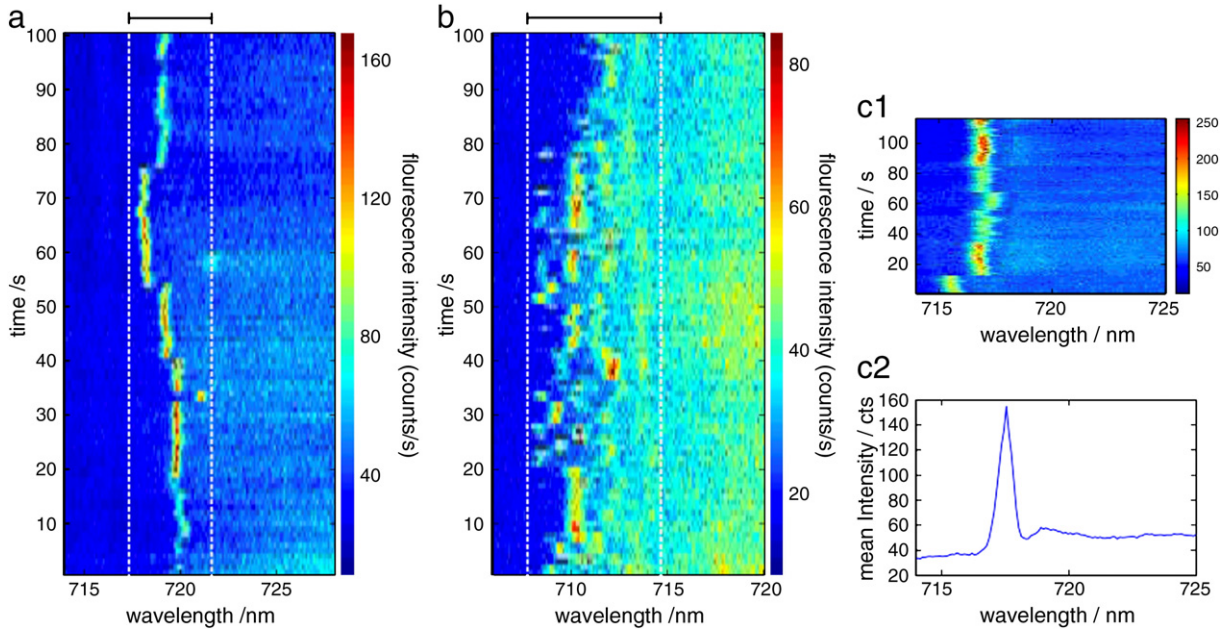


**Fig. 4.** (a, b) Sequence of 100 fluorescence spectra of two different single PSI trimers from *A. platensis* measured continuously with an acquisition time of 1 s for each spectrum; $\lambda_{exc} = 680$ nm, and T = 1.4 K. Fluorescence intensity is color-coded (see color code to the right of graphs). The spectral diffusion of the ZPLs is restricted to the wavelength range indicated by the white vertical dashed lines. (c1) Sequence of 120 fluorescence spectra of a single PSI trimer, where the ZPL resides almost on the same wavelength position. (c2) Average spectrum obtained by summation of all spectra depicted in (c1). Prior to that, each spectrum was shifted, so that the ZPL position is the same in each spectrum.

a spectral position for a shorter amount of time than the acquisition time two or more spectral positions are observed. In addition to the spectral variations, intensity changes of the ZPLs were observed. Such intensity changes are visible for both single PSI complexes (Fig. 4a and b). In Fig. 4a, after 20 s the ZPL intensity suddenly increases by factor >2 and after 76 s it decreases again. In Fig. 4b, intensity changes occur from second to second. In summary, ZPLs show dynamical variations of their spectral position and intensity. The rate and extent of these variations differ from complex to complex, but the ZPLs generally remain in confined spectral regions. For the two examples in Fig. 4a and b these regions are illustrated by white dashed lines. Although, it is possible to resolve single ZPLs in those sequences, the observation of their phonon wings (PWs) is challenging and thus the determination of the electron–phonon coupling. The determination of the shape of the PW is hindered by two points. First, the intensity of the PWs is low and therefore an averaging of the data for at least several seconds is required; second, the shape of phonon wings is often distorted by other emitters. This makes it difficult to resolve the PWs. As a consequence, the determination of the ZPL together with its PW is only possible, if the emission is stable and if the background signals can be separated. In Fig. 4c1, such type of ZPL/PW couple is shown. The emission of this ZPL is only slightly disturbed by other emitters. In such a case it is possible to determine the shape of the ZPL and its PW. For this purpose, the mean position of the ZPL in the shown data-set was determined. After that, all spectra were shifted by $\Delta\lambda$ until the ZPL position matches the mean position. Then, the shifted spectra were averaged as shown in Fig. 4c2. Note: The original wavelength scale is no longer valid after shifting the spectra. In this case it is more appropriate to give an energy scale related to the position of the ZPL. Due to the small shifts $\Delta\lambda$, the original wavelength scale was maintained for convenience. In the average spectrum shown in Fig. 4c2, the ZPL with its accompanying phonon wing is visible. The slight bending of the baseline is due to small background contributions. Based on the intensity the Huang–Rhys factor S defining the strength of the electron phonon coupling can be calculated from $e^{-S} = \frac{I_{ZPL}}{I_{ZPL}+I_{PW}}$. $I_{ZPL}$ and $I_{PW}$ are the intensities of the ZPL and the phonon wing, respectively. For this line profile we deduce $S = 0.30 \pm 0.05$. In a second data-set, we obtained – by the same procedure – $S = 0.35 \pm 0.05$ (data not shown). Both values indicate weak electron–phonon coupling ($S < 0.7$) for the red states characterized by the occurrence of ZPLs.

### 3.3. Spectral distribution of ZPLs

Spectral positions of the ZPLs were determined for all 106 individual trimers automatically with the algorithm described in Materials and methods (Section 2.2). This algorithm is specially designed to detect ZPLs within noisy spectra taken in rapid succession. It accounts for their wavelength position, their dynamics, and occurrence. The histogram (Fig. 5) shows the distribution of the spectral positions of the ZPLs together with the average spectrum from Fig. 1. Using an automated evaluation method opens the possibility to compare the ZPL distributions for different types of sample preparation as well as among different organisms [27]. In addition, observing changes in the shape of the ZPL distribution opens the possibility to draw conclusions about the environment of the involved chromophore assemblies [21,27,28].

The ZPL distribution shown in Fig. 5 reveals the occurrence of ZPLs in the wavelength range between $\lambda > 696$ nm, which corresponds to the edge of the used long-pass filter (AHF HQ695LP) and 740 nm. The contributions between 708 and 718 nm dominate the distribution of ZPLs; their maximum is found at 714 nm and its FWHM is 6 nm. With few exceptions, all PSI trimers exhibit ZPLs in this band.

### 3.4. Assignment of spectral components

Further details about the emitters responsible for the far-red emission of PSI from *A. platensis* are obtained from the analysis of its polarization [25]. In Fig. 6 the emission of a single PSI trimer in dependence of the polarizer angle in front of the spectrograph is shown. The turning angle of the polarizer is defined with respect to an arbitrary laboratory axis and is uncorrelated to the polarization of the excitation light. The data set chosen for Fig. 6 shows the emission of a particular complex in which the otherwise dominant emitter at ≅730 nm is in a dark state (data not shown). In that case, the remaining emission was dominated by the far-red contribution as visible in the average spectrum given on top of Fig. 6. Overall, three contributions are clearly distinguishable: one broad emission at ≅730 nm, one ZPL at ≅732 nm and a

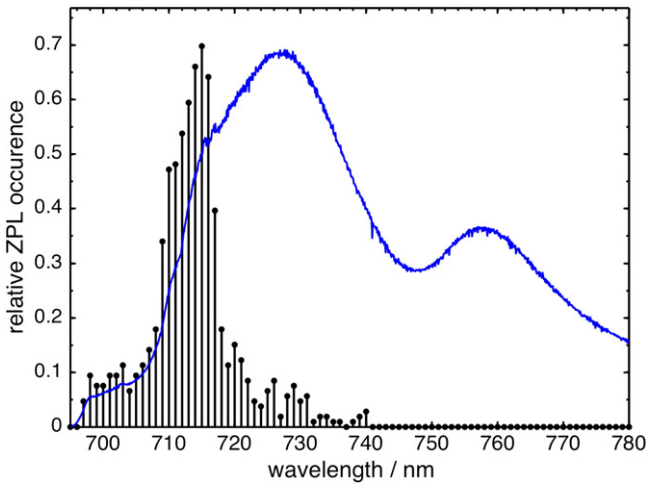


**Fig. 5.** ZPL histogram for PSI trimers from *A. platensis*. The histogram results from an algorithm applied to fluorescence spectra of single PSI trimers taken in rapid succession (for details see Material and methods). In addition, the average spectrum from Fig. 1 is given.

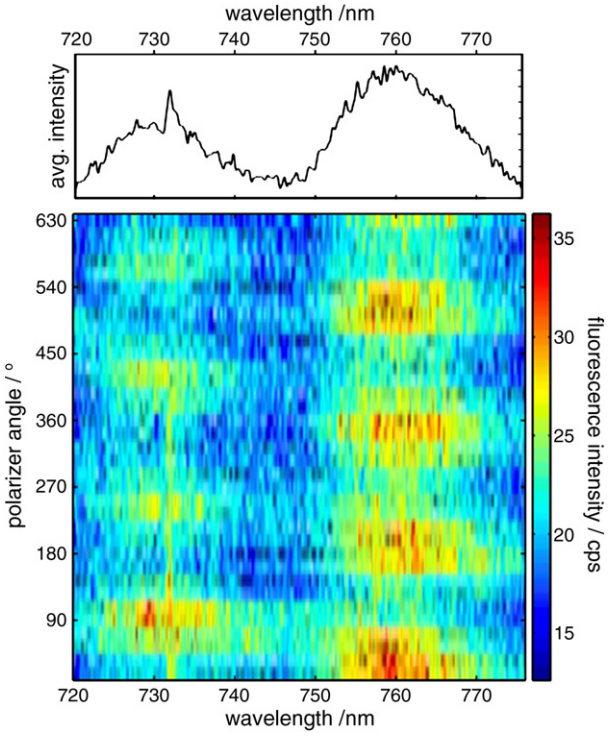


**Fig. 6.** Sequence of fluorescence spectra of a single PSI trimer as a function of the orientation of the polarizer in front of the spectrograph. The acquisition time was 1 s for each spectrum; $\lambda_{exc} = 680$ nm, and $T = 1.4$ K. The individual spectra were recorded while the polarizer was moving continuously with speed of 360°/20 s. The fluorescence intensity is encoded in the color scale on the right. The average fluorescence intensity is given on top. The data set chosen shows the emission of a single complex after the dominate emitters at ≅730 nm is in a dark state.

broad contribution at ≅760 nm. All contributions show modulation of their intensity in dependence of the turning of the polarizer. The intensity modulation of the broad contributions shows a clear sine waveform, whereas the intensity modulation of the ZPL is overlaid by a general intensity reduction. The fluorescence intensities of the broad contributions show a shift in phase by almost 80°. It should be noted that the obtained angle is not identical with the angle between the dipolar moments of the optical transitions of the two emitters. The value represents the angle between the projections of the transition dipole-moments into the image plane of the microscope objective.

## 4. Discussion

### *4.1. Comparison of the average spectra from single PSI trimers with ensemble data*

The absorbance of PSI trimers of *A. platensis* shows two main bands in the range >700 nm, they are named C708 and C740 in accordance with their maximum positions. Both bands are broad and the numbers of Chl molecules involved are 7–8 for C708 and 3 for C740 [6–8,12]. The details of the spectral classification are summarized in Table 1.

The fluorescence emission of PSI is a superposition of contributions from several red pool emitters. For PSI from *A. platensis* three contributions with maxima at 726 nm (F726), 731 nm (F731) and 760 nm (F760) were reported. The intensities of these contributions depend on the redox state of P700. In the reduced form of P700, the fluorescence spectrum is dominated by the emission of F760 [10,13]. If P700 becomes oxidized, F760 is strongly quenched. The emission spectrum is then dominated by F726 and F760 remains as a shoulder at the low energy side. Recent experiments on monomers of PSI from *A. platensis* gave evidence that F731 contributing to the broad band around 726 nm, is also quenched by $P700^+$ [13].

The single-molecule data presented here are collected with an excitation power of 100 μW. First, we have to account for the oxidation state of P700 during the single-molecule experiments. At low temperature, the highest rate for the recovery of the ground state of P700 is achieved in centers with prereduced iron-sulfur clusters $F_A$ and $F_B$. Under these conditions, the radical pair $P700^+A_1^-$is formed which decays by charge recombination with a half-life of 170 μs [29]. At the excitation power used, the excitation rate is significantly higher than $(170\,\mu s)^{-1}$ and P700 is for >99% of the time in the oxidized state [13]. As a consequence, it should be expected that F731 and F760 are quenched by $P700^+$. In Fig. 1, the average spectrum obtained from the summation of the emission from single PSI trimers is shown. The spectrum shows a maximum at about 725 nm and a shoulder at ≅760 nm. The shape of the spectrum is similar to the ensemble spectra of trimeric PSI with oxidized P700. Thus, the visible contributions can be associated with the respective long-wavelength Chls F726 and F760. The polarization dependent data (Fig. 6) give additional evidence that the emission of F726 and F760 is due to individual broad emitters. The complete band associated with F760 (here 750–770 nm) undergoes a uniform modulation while turning the polarizer. The uniform modulation can be explained with a single emitter constituting F760 that is able to cover almost the whole width of the F760 emission. The behavior is similar for the emitter giving rise for the broad band around 726 nm.

At low temperatures, the presence of a ZPL is a characteristic feature for the emission of single emitters, but in the spectral range of F726 only a very small number of ZPLs are observed; and for F760 no ZPLs are observed at all. The invisibility of ZPLs is possible, if the intensity of the ZPLs falls below the noise level. The intensity of the ZPL depends on the strength of the electron–phonon coupling. If the electron–phonon coupling gets stronger, the intensity of the ZPL shrinks at the expense of its phonon wing (see Fig. 1 in Ref. [28]). A complete disappearance of the ZPLs as observed for the emission of F760 becomes only possible for very strong electron–phonon coupling or for spectral diffusion on a time scale faster than the acquisition time or for a combination of both processes. Without broadening by spectral diffusion, a value of S≥5 is required at the S/N ratio of the spectra shown in Fig. 1 of Ref. [28]. The observed Stokes-shift of about 20 nm (~350 $cm^{-1}$) for the reddest emitter (absorption around 740 nm and emission around 760 nm) supports the assumption of a very strong electron–phonon coupling for C740/F760. Stark spectroscopy revealed very large polarizability differences and permanent dipole changes between the ground and excited state, which are about a factor of 3 to 5 larger than that of monomeric Chl [19,33] for the red-most states C740 in *A. platensis* and C719 in *T. elongatus*. These unusual spectroscopic properties provide evidence that strongly excitonically coupled Chls are responsible for the long wavelength absorption and emission, respectively. Indeed, the very large polarizability differences of the red-most states, which is similar to those of the special pair of the purple bacterial reaction center, indicates the mixing of charge transfer states into the excited excitonic state. This could explain the strong electron–phonon coupling.

In the spectral range of F726 a small number of ZPLs was observed (see Fig. 5). In this case, a combination of fast spectral diffusion with an electron–phonon coupling in the range of ≅2.9 is most likely the reason for the broad unstructured band similar to the results obtained with LWCs in PSI of *Synechocystis* sp. PCC 6803 [28].

In the wavelength region between 710 and 740 nm another emitter belonging to the C708 pool was observed with quite different spectral properties. This red state could be detected by its zero-phonon lines. The center of the zero-phonon line distribution is found at ≅714 nm, the Huang–Rhys factor has been estimated to be about 0.3. Accordingly, this red state has its absorption on the long-wavelength side of the absorption band assigned to the C708 pool.

### *4.2. ZPL distributions of PSI from A. platensis and T. elongatus are similar*

The average spectrum given in Fig. 1 shows a slight shoulder in the region ≅715 nm. This shoulder is due to a weak emitter observable by prominent ZPLs (Fig. 3) in the spectra of single PSI trimers. Compared to data from ensemble spectroscopy [13], the shoulder is here more pronounced. As shown recently for PSI of *T. elongatus*, the reason for the variation of the intensity is based on the different amount of glycerol that is added during sample preparation [27]. As shown in Figs. 3 and 4, these ZPLs undergo spectral diffusion. The rates of the spectral diffusion processes vary from ZPL to ZPL as shown in Fig. 3. In many cases, the rate of the site energy changes remains below the rate of data acquisition (≅1 s). Then the time-dependent diffusion of those ZPLs can be observed as spectral trails (Fig. 4). The spectral diffusion properties depend on the flexibility of the chromophore bound to the protein [21,27]. The fluorescence emission of the LWCs of PSI is a perfect example. Some contributions show sharp ZPLs, some show broad intensity distributions. However, all rely on Chl aggregates with strong excitonic coupling located in different protein environments. The spectral trails observed in PSI from *A. platensis* show a high similarity with the time-dependent movement of ZPLs observed for PSI from *T. elongatus* [21,27]. Furthermore, the occurrence of ZPLs in the data of single PSI trimers from *A. platensis* and *T. elongatus* shows in both cases a distribution with well-defined maximum located at 714 nm for PSI from *A. platensis* (Fig. 5) and at 710 nm for PSI of *T. elongatus* [21,27]. The spectral diffusion properties and the wavelength position of these ZPLs are in reasonable agreement. As a consequence, it is most likely that structure and the binding situation of the Chl*a* aggregate responsible for the ZPLs in *A. platensis* and in *T. elongatus* is similar.

### *4.3. The red states emitting at 726 and 760 nm are not connected via energy transfer at cryogenic temperatures*

If fast energy transfer would lead to thermal equilibration of excitation energy in the antenna, the localization of the excited singlet

state on C740 over C708 is favored by the Boltzmann factor $\exp(-\Delta E/kT)$, where $\Delta E$ is the difference between the excitation energies of C708 and C740. This factor is about 19, even at room temperature, whereas at 1.4 K it would be a factor of about $10^{272}$. Therefore, the excitation energy would be exclusively trapped on the reddest state C740. As a consequence, fluorescence would be emitted only from the long-wavelength Chl with the lowest energy between ground and excited state. Since fluorescence is observed at 1.4 K from several LWC emitters (see Fig. 1), it can be concluded that the excitation energy is trapped at different red states, which are not connected by fast energy transfer.

This conclusion is supported by Fig. 2b. The intensity ratio $I_{max}(F726)/I_{max}(F760)$ is plotted against the wavelength difference of the peak positions ($\Delta\lambda = \lambda_{F760} - \lambda_{F726}$) determined for all emission spectra of single PSI trimers. The spectral separation $\Delta\lambda$ varies in the range 18–44 nm. The variation of $\Delta\lambda$ should have an effect on the spectral overlap and thus also on the rate of energy transfer between these long-wavelength forms. For high energy transfer rates one would expect a low value of $I_{max}(F726)/I_{max}(F760)$. The emission around 760 nm (F760) can be associated with an emitter absorbing around 740 nm (C740) indicating a Stokes-shift of about 20 nm. The maximal spectral overlap between donor and emitter is expected, if the maximum of the emission of F726 and the absorption of F760 overlaps. With a Stokes-shift of 20 nm for F760, this is realized if the emission of F726 and F760 separated by about $\Delta\lambda \cong 20$ nm. Fig. 2b shows, however, that there is no correlation between the intensity ratio and the value of $\Delta\lambda$ indicating that energy transfer from F726 to F760 does not occur or more precisely that the transfer is slow compared to the intrinsic decay time of the excited singlet state of the emitter F726. A similar behavior was observed in PSI of *T. elongatus;* it was shown that Chls excited at 730 nm no longer transfer their energy to neighboring Chls [30].

According to Förster theory, the rate of energy transfer between two chromophores depends on (a) the distance between donor and acceptor, (b) the spectral overlap between the emission spectrum of the donor and the absorption spectrum of the acceptor and, (c) the orientation factor for the dipole–dipole interaction.

The absence of energy transfer from C708 to C740 can be due to the large distance between the different Chl aggregates responsible for the emission at 726 nm and 760 nm or due to an almost perpendicular orientation of their transition dipole moments. This observation can be discussed on the basis of the proposed candidates for F726 and F760. Although the structure of PSI from *A. platensis* is unknown, it is reasonable to assume a high similarity of the structural organization of PSI from *A. platensis* and *T. elongatus*. The Chl aggregate A31–A32–B7 in the trimerization domain is most likely responsible for F760 [13]. For F726 several candidates are discussed. Among others, the most likely candidates are: B37–B38, A38–A39, B18–B19, and A16–A17–A25. These Chl aggregates meet three necessary conditions: strong coupling between the chlorophylls of the aggregate (see Table 3 in Ref. [31]), orientation of the transition dipole of the low-energy exciton state parallel to the membrane plane [32] and, finally, a large distance to P700 [2]. These aggregates might be responsible for F726. The distance between A31–A32–B7 and the candidates for F726 are: d(A31–A32–B7 – B37–B38) ≅22 Å, d(A31–A32–B7 – A38–A39)≅57 Å, d(A31–A32–B7 – B18–B19)≅52 Å, and d(A31–A32–B7 – A16–A17–A25)≅48 Å. These distances are all smaller than the Förster radius that defines the distance for which the rate of energy transfer becomes equal to the intrinsic rate of radiative decay. For Chls with identical $Q_Y$ transition energies, a value of $R_0 = 65$ Å [34] has been estimated. Therefore an exclusion based on the distance is not possible. Consequently, the orientation factor might be responsible for the missing transfer. Unfortunately, the orientation of the transition dipole moment of tightly coupled Chls can deviate remarkably from an estimation that is based on a simple dipole–dipole model. Therefore, the determination of the lowest exciton state and its orientation calculated from a more sophisticated theoretical approach is required for this type of analysis.

### 4.4. Comparison of the red states in PSI from A. platensis and T. elongatus

The absorption and the emission spectra of PSI of *A. platensis* and *T. elongatus* show remarkable differences. The most striking difference of the absorption spectra is found in the wavelength range >700 nm. For PSI of *A. platensis* two well resolved contributions at ≅710 nm and ≅740 nm are observed, whereas the absorption of *T. elongatus* shows only one defined maximum at ≅708 nm together with a broad shoulder around 720 nm. The difference between the fluorescence emission spectra is even more striking. For PSI of *A. platensis,* two well resolved bands at ≅730 nm and ≅760 nm are present, whereas in *T. elongatus* just one broad band is observed. Nevertheless, recent experiments on PSI trimers and monomers of both cyanobacteria revealed remarkable similarities between the long-wavelength Chls [13]. By these experiments, it became obvious that the most-red emitter is strongly quenched by $P700^+$ both in PSI of *A. platensis* (F760) and in *T. elongatus* (F739). In each case, the responsible emitters show a Stokes-shift of almost 20 nm. The absorbance (C740/C719) and the emission (F760/F739) of these red Chls is lost in PSI monomers. Thus, a localization of the aggregate in the trimerization domain is most likely and a high structural similarity between the arrangements of the maximum long-wavelength chlorophylls is obvious. A similar formation of a long-wavelength state was observed between the complexes in PSI-LHCI [35]. The only remaining difference between these reddest Chls is the difference of almost 20 nm in their absorption wavelength. The reason for this shift remains unclear. Further similarities are observed for the emission in the range of 730 nm. This part of the emission of *A. platensis* is composed of at least two independent contributions, named F726 and F731. A similar composition of contributions is found for PSI from *T. elongatus*, there the two contributions were named F730 and F734. The more red-shifted pools (F731/F734) exhibit strong quenching by $P700^+$. Consequently, both emitters must be located in the vicinity of P700. The fluorescence emission of PSI with oxidized P700 is due to the remaining F726 or F731, respectively. At the single-molecule level, the fluorescence emission of these emitters shows broad intensity distributions due to a combination of spectral diffusion and increased electron–phonon coupling [36]. Based on the insensitivity of F726/F731 on the redox state of P700, their comparable wavelength position, spectral diffusion properties and electron–phonon coupling, a high similarity between the responsible Chl aggregates in PSI of *A. platensis* and *T. elongatus* can be assumed.

Besides the already discussed similarities, the observation of sharp ZPLs in the wavelength range <720 nm of single PSI trimers of both organisms is striking. Based on the similarities of these ZPLs also a high structural analogy between PSI from *A. platensis* and *T. elongatus* can be expected. As a consequence, the absorption of the contributions responsible for the ZPLs and for F726 (*A. platensis*) or F730 (*T. elongatus*) must originate from C708.

## 5. Conclusions

The fluorescence emission spectra of single PSI trimers from *A. platensis* are composed of sharp ZPLs and broad intensity distributions. The ZPLs distributed around 714 nm can be assigned to red states belonging to C708. The broad fluorescence bands at ≅726 and ≅760 nm are individual emitters that are broadened by strong electron–phonon coupling and rapid spectral diffusion. The transfer of excitation energy between Chl aggregates associated with F726 and F760 seems to be negligible, although all possible candidates are close enough for energy transfer. Therefore, an almost perpendicular orientation of the transition dipole moments of F726 and F760 can be assumed. Summarizing, the results from the single-molecule level with recent experiments at the ensemble level reveal that the different red Chl in PSI from *A. platensis* and *T. elongatus* rely on several Chl aggregates with comparable properties.

## Acknowledgements

Single-molecule experiments were carried out in the laboratory of Prof. Robert Bittl (Free University Berlin); his continuous support is gratefully acknowledged. Volker Radics is gratefully acknowledged for technical advice and assistance during the measurements. Financial support from the German Research Council, DFG (SFB 498, TP A6, E.S.) and by Heisenberg-Program (BR 4102/1-1 and BR 4102/2-1), the Russian Academy of Sciences, program MCB and RFBR (Grant 11-04-00247a, to N.V.K.) is gratefully acknowledged.

## References

[1] J.H. Golbeck (Ed.), Photosystem I: The Light-Driven Plastocyanin:Ferredoxin Oxidoreductase, Springer, 2006.
[2] P. Jordan, P. Fromme, H.T. Witt, O. Klukas, W. Saenger, N. Krauss, Three-dimensional structure of cyanobacterial photosystem I at 2.5-Angstrom resolution, Nature 411 (2001) 909–917.
[3] P. Fromme, P. Jordan, N. Krauss, Structure of photosystem I, Biochim. Biophys. Acta 1507 (2001) 5–31.
[4] A. Ben-Shem, F. Frolow, N. Nelson, Crystal structure of plant photosystem I, Nature 426 (2003) 630–635.
[5] M.K. Sener, C. Jolley, A. Ben-Shem, P. Fromme, N. Nelson, R. Croce, K. Schulten, Comparison of the light-harvesting networks of plant and cyanobacterial photosystem I, Biophys. J. 89 (2005) 1630–1642.
[6] N.V. Karapetyan, A.R. Holzwarth, M. Rögner, The photosystem I trimer of cyanobacteria: molecular organization, excitation dynamics and physiological significance, FEBS Lett. 460 (1999) 395–400.
[7] N.V. Karapetyan, E. Schlodder, R. van Grondelle, J.P. Dekker, The long wavelength chlorophylls in photosystem I, in: J.H. Golbeck (Ed.), The Light-Driven Plastocyanin: Ferredoxin Oxidoreductase, Advances in Photosynthesis and Respiration vol. 24, Photosystem I: The Light-Driven Plastocyanin:Ferredoxin Oxidoreductase, Springer, 2006, pp. 177–192.
[8] B. Gobets, R. van Grondelle, Energy transfer and trapping in photosystem I, Biochim. Biophys. Acta 1507 (2001) 80–99.
[9] L.O. Palsson, C. Flemming, B. Gobets, R. van Grondelle, J.P. Dekker, E. Schlodder, Energy transfer and charge separation in photosystem I: P700 oxidation upon selective excitation of the long-wavelength antenna chlorophylls of *Synechococcus elongatus*, Biophys. J. 74 (1998) 2611–2622.
[10] V.V. Shubin, I.N. Bezsmertnaya, N.V. Karapetyan, Isolation from *Spirulina* membranes of two photosystem I-type complexes, one of which contains chlorophyll responsible for the 77-K fluorescence band at 760 nm, FEBS Lett. 309 (1992) 340–342.
[11] V.V. Shubin, V.L. Tsuprun, I.N. Bezsmertnaya, N.V. Karapetyan, Trimeric forms of the photosystem-I reaction-center complex pre-exist in the membranes of the cyanobacterium *Spirulina platensis*, FEBS Lett. 334 (1993) 79–82.
[12] E. Schlodder, M. Cetin, M. Byrdin, I.V. Terekhova, N.V. Karapetyan, $P700^+$- and $^3P700$-induced quenching of the fluorescence at 760 nm in trimeric photosystem I complexes from the cyanobactenium *Arthrospira platensis*, Biochim. Biophys. Acta 1706 (2005) 53–67.
[13] E. Schlodder, M. Hussels, M. Cetin, N.V. Karaperyan, M. Brecht, Fluorescence of the various red antenna states in photosystem I complexes from cyanobacteria is affected differently by the redox state of P700, Biochim. Biophys. Acta 1807 (2011) 1423–1431.
[14] J. Kruip, N.V. Karapetyan, I.V. Terekhova, M. Rögner, In vitro oligomerization of a membrane protein complex — liposome-based reconstitution of trimeric photosystem I from isolated monomers, J. Biol. Chem. 274 (1999) 18181–18188.
[15] N.V. Karapetyan, V.V. Shubin, R.J. Strasser, Energy exchange between the chlorophyll antennae of monomeric subunits within the Photosystem I trimeric complex of the cyanobacterium *Spirulina*, Photosynth. Res. 61 (1999) 291–301.
[16] N.V. Karapetyan, D. Dorra, G. Schweitzer, I.N. Bezsmertnaya, A.R. Holzwarth, Fluorescence spectroscopy of the longwave chlorophylls in trimeric and monomeric photosystem I core complexes from the cyanobacterium *Spirulina platensis*, Biochemistry 36 (1997) 13830–13837.
[17] V.V. Shubin, I.N. Bezsmertnaya, N.V. Karapetyan, Efficient energy-transfer from the long-wavelength antenna chlorophylls to P700 in photosystem-I complexes from *Spirulina platensis*, J. Photochem. Photobiol. B 30 (1995) 153–160.
[18] N. Krauss, W.D. Schubert, O. Klukas, P. Fromme, H.T. Witt, W. Sänger, Photosystem I at 4-Å resolution represents the first structural model of a joint photosynthetic reaction centre and core antenna system, Nat. Struct. Biol. 3 (1996) 965–973.
[19] V. Zazubovich, S. Matsuzaki, T.W. Johnson, J.M. Hayes, P.R. Chitnis, G.J. Small, Red antenna states of photosystem I from cyanobacterium *Synechococcus elongatus*: a spectral hole burning study, Chem. Phys. 275 (2002) 47–59.
[20] F. Jelezko, C. Tietz, U. Gerken, J. Wrachtrup, R. Bittl, Single-molecule spectroscopy on photosystem I pigment–protein complexes, J. Phys. Chem. B 104 (2000) 8093–8096.
[21] M. Brecht, H. Studier, A.F. Elli, F. Jelezko, R. Bittl, Assignment of red antenna states in photosystem I from *Thermosynechoccocus elongatus* by single-molecule spectroscopy, Biochemistry 46 (2007) 799–806.
[22] P. Tamarat, A. Maali, B. Lounis, M. Orrit, Ten years of single-molecule spectroscopy, J. Phys. Chem. A 104 (2000) 1–16.
[23] C. Hofmann, T.J. Aartsma, H. Michel, J. Köhler, Direct observation of tiers in the energy landscape of a chromoprotein: a single-molecule study, Proc. Nat. Acad. Sci. U. S. A. 100 (2003) 15534–15538.
[24] S. Krause, P.F. Aramendia, D. Tauber, C. von Borczyskowski, Freezing single molecule dynamics on interfaces and in polymers, Phys. Chem. Chem. Phys. 13 (2011) 1754–1761.
[25] A.F. Elli, F. Jelezko, C. Tietz, H. Studier, M. Brecht, R. Bittl, J. Wrachtrup, Red pool chlorophylls of photosystem I of the cyanobacterium *Thermosynechococcus elongatus*: a single-molecule study, Biochemistry 45 (2006) 1454–1458.
[26] F. Müh, A. Zouni, Micelle formation in the presence of photosystem I, Biochim. Biophys. Acta 1778 (2008) 2298–2307.
[27] M. Hussels, M. Brecht, Effect of glycerol and PVA on the conformation of photosystem I, Biochemistry 50 (2011) 3628–3637.
[28] M. Brecht, H. Studier, V. Radics, J.B. Nieder, R. Bittl, Spectral diffusion induced by proton dynamics in pigment–protein complexes, JACS 130 (51) (2008) 17487–17493.
[29] E. Schlodder, K. Falkenberg, M. Gergeleit, K. Brettel, Temperature dependence of forward and reverse electron transfer from $A_1^-$, the reduced secondary electron acceptor in photosystem I, Biochemistry 37 (1998) 9466–9476.
[30] L.O. Palsson, J.P. Dekker, E. Schlodder, R. Monshouwer, R. van Grondelle, Polarized site-selective fluorescence spectroscopy of the long-wavelength emitting chlorophylls in isolated photosystem I particles of *Synechococcus elongatus*, Photosynth. Res. 48 (1996) 239–246.
[31] M. Byrdin, P. Jordan, N. Krauss, P. Fromme, D. Stehlik, E. Schlodder, Light harvesting in photosystem I: modeling based on the 2.5-Angstrom structure of photosystem I from *Synechococcus elongatus*, Biophys. J. 83 (2002) 433–457.
[32] E. Schlodder, V.V. Shubin, E. El-Mohsnwy, M. Rögner, N.V. Karapetyan, Steady-state and transient polarized absorption spectroscopy of photosystem I complexes from the cyanobacteria *Arthrospira platensis* and *Thermosynechococcus elongatus*, Biochim. Biophys. Acta - Bioenerg. 1767 (6) (2007) 732–741.
[33] R.N. Frese, M.A. Palacios, A. Azzizi, I.H.M. van Stokkum, J. Kruip, M. Rögner, N.V. Karapetyan, E. Schlodder, R. van Grondelle, J.P. Dekker, Electric field effects on red chlorophylls, beta-carotenes and P700 in cyanobacterial photosystem I complexes, Biochim. Biophys. Acta 1554 (2002) 180–191.
[34] K. Colbow, Energy transfer in photosynthesis, Biochim. Biophys. Acta 314 (1973) 320–327.
[35] R.C. Jennings, G. Zucchelli, E. Engelmann, F.M. Garlaschi, The long-wavelength chlorophyll states of plant LHCI at room temperature: a comparison with PSI-LHCI, Biophys. J. 87 (2004) 488–497.
[36] R. Croce, G. Zucchelli, F.M. Garlaschi, R.C. Jennings, A thermal broadening study of the antenna chlorophylls in PSI-200, LHCI, and PSI core, Biochemistry 37 (1998) 17355–17360.
[37] M. Ratsep, T.W. Johnson, P.R. Chitnis, G.J. Small, The red-absorbing chlorophyll a antenna states of photosystem I: a hole-burning study of *Synechocystis sp* PCC 6803 and its mutants, J. Phys. Chem. B 104 (2000) 836–847.
[38] M. Brecht, V. Radics, J.B. Nieder, H. Studier, R. Bittl, Red antenna states of photosystem I from *Synechocystis* PCC 6803, Biochemistry 47 (2008) 5536–5543.
[39] M. Brecht, J.B. Nieder, H. Studier, E. Schlodder, R. Bittl, Red antenna states of photosystem I from *Synechococcus sp.* PCC 7002, Photosynth. Res. 95 (2008) 155–162.